

# We are IntechOpen, the world's leading publisher of Open Access books Built by scientists, for scientists

6,900

Open access books available

185,000

International authors and editors

200M

Downloads

Our authors are among the

154

Countries delivered to

TOP 1%

most cited scientists

12.2%

Contributors from top 500 universities



WEB OF SCIENCE™

Selection of our books indexed in the Book Citation Index  
in Web of Science™ Core Collection (BKCI)

Interested in publishing with us?  
Contact [book.department@intechopen.com](mailto:book.department@intechopen.com)

Numbers displayed above are based on latest data collected.  
For more information visit [www.intechopen.com](http://www.intechopen.com)



---

# Pure 7000 Alloys: Microstructure, Heat Treatments and Hot Working

---

P. Leo and E. Cerri

Additional information is available at the end of the chapter

<http://dx.doi.org/10.5772/3354>

---

## 1. Introduction

7000 alloys are used above all in automotive industry and architectural applications. These materials exhibit medium strength and ductility at room temperature and can be strengthened by aging treatment. Moreover they are characterized by low quench sensitivity, good corrosion resistance (due to the absence of Cu addition) and good extrudability (higher than 6061 alloy) [1-5].

Because of their commercial importance, much effort has been spent on investigation of the precipitation process in Al-Zn-Mg alloys [6-10]. The high strength exhibited in the hardened state is due to a fine distributions of precipitates, notably of the metastable  $\eta'$  phase  $MgZn_2$ , produced by artificial aging from a supersaturated solid solution. The temperature of artificial aging influences the kinetics and the sequence of precipitation and if heterogeneous nucleation of the equilibrium phase appears, a less efficient hardening is obtained. In this study the response to artificial aging with and without previous solution treatment has been analyzed in the range of 130°C-210°C in order to evaluate which effect on hardening is due to the absence of supersaturation of vacancy rich cluster (VRC) and alloying elements coming from a solution heat treatment and rapid quenching.

There is strong academic and industrial interest in recrystallization driven by the need to understand and control this phenomenon in order to optimize properties through the careful control of thermomechanical processing schedules [11]. In this paper, the effects of different heat treatments and Zr content on rate of recrystallization induced by annealing heat treatment after RT deformation and on further deformation in terms of strain hardening rate ( $SHR = d\sigma/d\varepsilon$ ), have been analyzed. Recrystallization due to hot deformation by torsion and tension test at 200°C-500°C and  $10^{-5}s^{-1}$ - $10^{-3}s^{-1}$  has been investigated too. During hot working the Al-Zn-Mg alloys exhibit lower flow stress and higher ductility than Al-Mg alloy (for ex-

ample 5182 and 5083) [12,13]. Generally dynamic recovery (DRV) is the sole restoration mechanism in Al alloys [14-17] developing a subgrain structure inside elongated grain. As a consequence, the flow curves (stress vs strain;  $\sigma$  vs  $\epsilon$ ) exhibit SH to a steady state regime, although adiabatic heating may cause a peak and a gradual softening particularly at high strain rate ( $\dot{\epsilon}$ ) and low temperature (T). Ductility is usually high because DRV softened grains allow accommodation of differential grain boundary (GB) sliding, slowing crack formation [18-22]. Solute, in the form of atmospheres hinder dislocation glide reducing DRV and ductility and raising the flow stress [21-23]. Moreover fine dispersoids pin dislocations and reduce DRV [24,25]. Precipitation hardening alloys may present varied behaviours as a result of changes in precipitate morphology. Growth of precipitates during hot working leads to good ductility and lower stress as shown for Al-Mg-Si [26,27], Al-Cu-Mg [28,29] and Al-Zn-Mg-Cu [30,31]. Solution treated alloy can exhibit high peak stress and dislocation density due to dynamic precipitation (DPN), followed by rapid softening as particles coalesce [29-33]. In this paper the microstructure of hot deformed Al-Zn-Mg samples (even modified with Zr) both by torsion and tension test have been analyzed by SEM and optical microscopy in order to justify the stress-strain curve shape.

Hot working of many engineering alloys is often accompanied by the formation of internal cavities [34-38]. The cavitation process depends strongly on alloy composition and microstructure as well as on the imposed processing condition [3 4 36 37 39]. Particularly large particles and inclusions, notably on GB, introduce new sources of fissure nucleation lowering ductility; solidification segregation and low melting constituents, especially if they spread along the GB, create severe problems [39]. Such cavitation may lead to premature failure (i.e. failure at strains lower than those expected based on material properties such as the strain rate sensitivity index and the strain hardening exponent) or result in a finished part with degraded mechanical properties. The cavitation process comprises three distinct stages, which in most cases occur simultaneously, i.e., (i) cavity nucleation, (ii) cavity growth, and (iii) cavity coalescence. Cavities, which usually nucleate preferentially at GB, triple points, or second-phase particles, grow by either plasticity- or diffusion-controlled mechanisms, or a combination of the two [35,37,39]. For a given material, the particular mechanism varies with the imposed deformation conditions.

## 2. Experimental procedures

The compositions of the alloys studied in this investigation are reported in Table1.

In order to distinguish easily the two materials with regard to Zr content they have been designated respectively as 7000 and 7000Zr. The materials were supplied in the form of DC cast billet of 20 cm in diameter and 40 cm in length. Cylindrical samples with gage length of 13 mm and 5mm diameter were cut parallel to the longitudinal axis of the billet for tensile and torsion tests. From the same billet, cube samples of 10 mm edges were cut for heat treatments. Artificial aging has been carried out at 130°C, 160°C, 190°C and 210°C up to 432h on the as-cast samples and 48h and solutionized ones (2h at 490°C). The ef-

fects of heat treatments were analyzed by hardness (HRF) and electrical conductivity curves.

	Zn	Mg	Fe	Si	Ti	Zr
7000	5.5	1.2	0.07	0.03	0.01	
7000Zr	5.6	1.2	0.07	0.03	0.01	0.16

**Table 1.** Composition of the alloys (wt%)

The microstructure of as-received alloys has been investigated by optical microscope (Nikon Epiphot 200) and Scanning Electron Microscope - Focused Ion Beam (SEM FIB) ZEISS 1540. The chemical composition of the matrix and particles was investigated by Energy-dispersive X-ray spectroscopy (EDS) analysis. For polarized light observation the samples were ground according to standard methods, electropolished (80ml perchloric acid, 120ml distilled water, 800ml ethanol, 20V) and anodized (Barker's reagent). The average grain size has been evaluated on a population of at least 200 grains by using the NIS software for imaging analysis.

RT tensile tests were performed on as-cast, solutionized (490°C-2h) and peak aged (490°C-2h + 160°C-24h) samples and SHR plotted versus ( $\sigma$ - $\sigma_y$ ). One half of each fractured sample coming from an RT tensile test was ground parallel to longitudinal axis up to the middle plane and annealed at 500°C for 3h. After 1,5 h of annealing, the sample was water quenched and the average grain size calculated in a fixed area close to the fracture by using the LUCIA G software. Then a second step of annealing at the same temperature and time (total 3h) was applied to each sample in order to follow the recrystallization behaviour.

Hot tensile tests have been performed on as-cast alloys in the range 250°C-400°C and  $10^{-5}$  to  $10^{-3}$  s<sup>-1</sup>. The temperature was measured by two independent thermocouples placed close to the sample. The true stress-true strain curves were calculated from recorded load-displacement data according to the usual formula. Hot torsion tests have been performed in the range 250°C-500°C and  $10^{-2}$  to  $5$  s<sup>-1</sup>. The torque and surface strain have been transformed into equivalent stress and strain by the traditional means. One half of each fractured sample coming from hot deformation tests were ground parallel to longitudinal axis up to the mid- plane in order to investigate on both recrystallization (RX) and cavitation phenomena by optical and SEM analysis. Particularly, for cavitation analysis, micrographs at 20× have been taken along the length of each metallographic section ( up to 4mm by fracture mid line) and collected into a montage [Fig.15 a,b,c]. The area of cavities inside the area of metallographic section (4mm by fracture mid line) and the same area of metallographic section has been evaluated using NIS software. Cavity area fractions Cs (%) (area of cavities divided by the area of metallographic section) were determined. Assum-

ing that cavities are randomly distributed inside the specimen, it has been shown that the area fraction is equal to volume fraction  $C_v$  (%) [30].

### 3. Results and discussion

The microstructures of as received alloys exhibit interdendritic segregation (Fig.1). In 7000 alloy (Fig 1a) the addition of small amount of Ti produces grain refining because the  $Al_3Ti$  particles act as nucleation sites and moreover lead to smaller precipitate free zones (PFZ) and finer grain boundary precipitation [43,44]. In 7000 Zr alloy (Fig 1b) the average grain size is higher compared to that of 7000 alloy ( $210 \pm 60 \mu m$  vs  $145 \pm 40 \mu m$ ). It is suggested that Zr reacts with  $Al_3Ti$  complex to make it a less potent nucleation site [44]. From SEM/ EDS analysis (Fig.2) hard insoluble brittle particles  $FeAl_3/FeAl_6$  type have been detected along grain boundaries (Fig.2a) and  $MgZn_2$  or  $Mg_3Zn_3Al_3$  both along and grain boundaries and inside grains (Fig.2b).

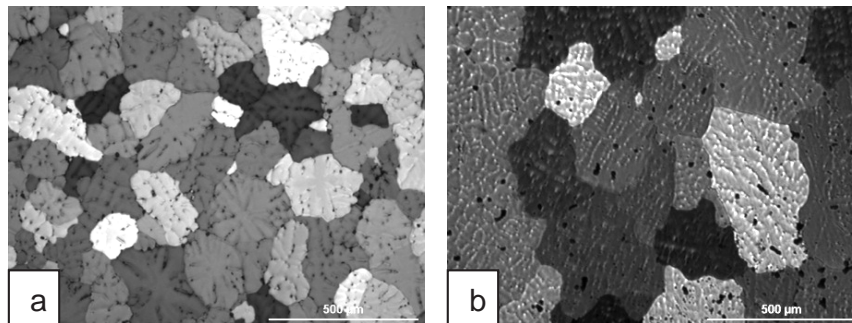


**Figure 1.** Optical micrographs of 7000 (a) and 7000Zr (b) alloys (5X) showing that the microstructure of both alloys is characterized by dendritic microsegregation. Different grain size is evident comparing (a) and (b)

The average values of hardness in the as-cast and solutionized state ( $490^\circ C-2h$ ) are slightly higher for 7000Zr alloy (Table 2) despite its grain size being higher. In contrast, the as-cast 7000Zr electrical conductivity is lower ( $22 Ms/m$  vs  $23,5 Ms/m$ ) for the higher amount of alloying. As shown in Fig.3 solution heat treatment ( $490^\circ C-2h$ ) reduce microsegregation and through dissolving hardening particles the hardness is reduced too (Table 2). EDS analysis did not find Al-Zn-Mg particles in solutionized alloys while some undissolved  $FeAl_3/FeAl_6$  type particles were found.

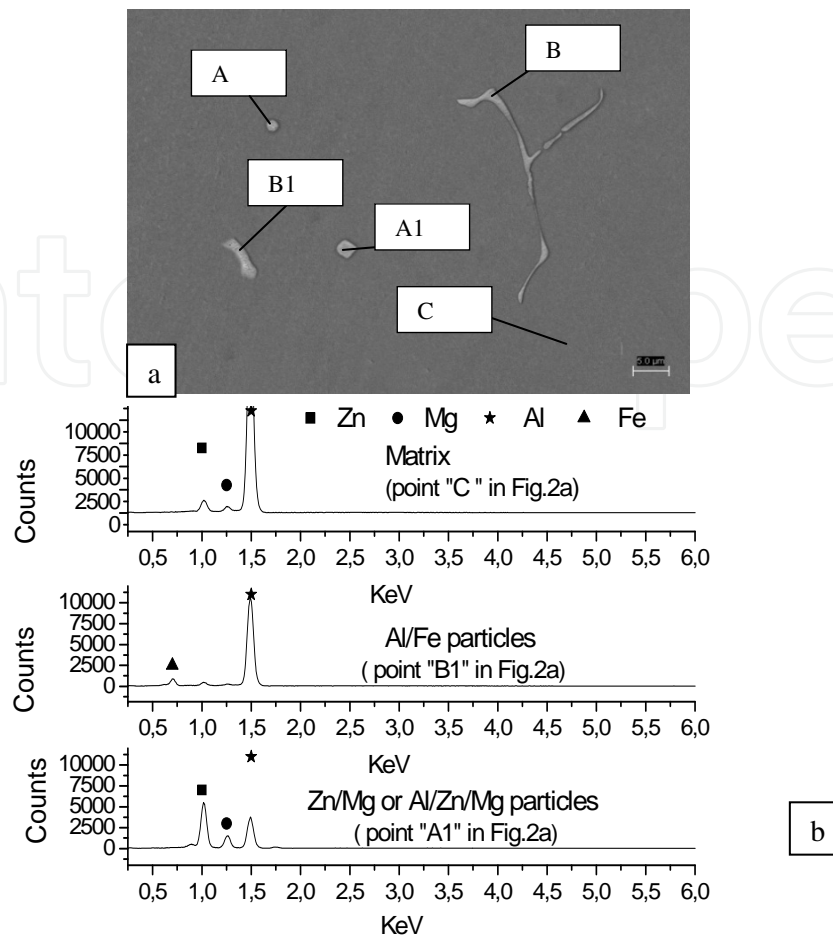


**Figure 2.** SEM micrograph showing Al/Fe particles (named B, B1) and particles containing Zn and Mg (named A,A1) (a); EDS spectrum of elements content (b) into the matrix (named C in Fig.2a), and B1 and A1 particles.

The hardness and electrical conductivity ageing curves performed on solution treated samples (T6 type) and on the as cast samples at 130-210°C are shown in Fig. 4 and Fig. 5 respectively. The aging treatments (Fig. 4) of solution treated (490°C-2h) samples lead to 15 and 13 point increments of hardness respectively for 7000 and 7000Zr at the two lowest temperatures of aging. At the higher temperatures, the precipitation kinetics are faster but the hardening is less efficient due to heterogeneous nucleations and overaging starts before the peak is reached. Moreover as the VRC are not retained at high temperature of aging, a lower density of hardening precipitates is expected. Comparing the behaviour of the two alloys, the response to T6 heat treatment is better at the higher temperature (190°C and 220°C) for the alloy containing Zr while it is similar for both alloys at the lower temperature of treatment. This behaviour could be due to Al<sub>3</sub>Zr compounds that don't dissolve at high temperature of treatment and act as nucleation sites for hardening precipitate η' phase [45-49]. The electrical conductivity increases with temperature of aging and time because of the draining of solute from the matrix as the precipitation process proceeds. The aging curves of the as cast samples (Fig. 5) do not show an increment of hardness with respect to the starting state. The absence of super saturation of VRC and alloying elements coming from a solution heat

treatment and rapid quenching, substantially reduces the nucleation of hardening precipitates. Even for this heat treatment the response of 7000Zr alloy is better at the higher temperature (190°C and 210°C) compared with the behavior of the alloy without Zr while it is similar for both alloys at the lower temperature of treatment. The electrical conductivity increases with temperature of aging and time but it is always lower than in the case of T6 heat treatment because of the lower supersaturation of the matrix.

	HRF As received	HRF Solutionized (490°C-2h)
7000	93	86
7000Zr	95	88

**Table 2.** HRF of as-cast and solutionized 7000 and 7000Zr alloy

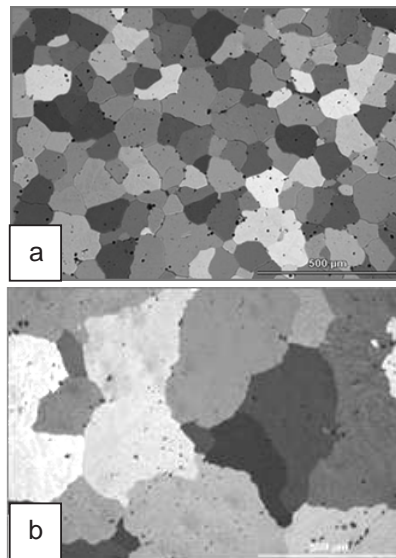


**Figure 3.** 7000 (a) and 7000Zr(b) alloys after solution heat treatment (490°C-2h). The dissolution of interdendritic segregation is evident compared to Fig.1

RT tensile tests on as-cast and solutionized samples indicate that solution heat treatment lead to low peak stress and high ductility (Fig.6) due to dissolution of both brittle phases and hardening particles. Moreover, the RT ductility is always higher for 7000Zr alloy. In term of SHR (Fig.7), it is always higher for the alloy in the as-cast state compared to solutionized because of large uncuttable particles cause Orowan hardening. Moreover 7000Zr alloy exhibits higher SHR probably due to the interaction of  $Al_3Zr$  particles with dislocations.

One half of each fractured samples was ground parallel to the longitudinal axis down to the mid plane and annealed at 500°C. After 1,5 h of annealing, the samples were water quenched and analyzed by optical microscopy for checking any recrystallization phenom-

ena. Then, a second step of annealing of 1,5h was applied to each sample (total 3h). Fig. 8 and Fig.9 illustrate the anodized microstructure of respectively 7000 and 7000Zr specimen as tensile tested (first line) and 3 hours annealed (second line). The first column presents pictures from the as cast sample, the second from the solution treated. Annealing treatment lead to recrystallization rate that is faster on as- cast alloys compared to the solutionized. This result can be clarified by considering that dissolved atoms and fine precipitates formed in the matrix limit the movement of dislocation during annealing and delay the nucleation and growth of new grains. The as cast alloy exhibits both the highest strain hardening rate and low dissolved atoms; both these aspects lead to a shorter recrystallization time. However as shown in Fig.9 the recrystallization of 7000Zr alloy is incomplete and not homogeneous even after three hours of annealing because of additions of Zr.

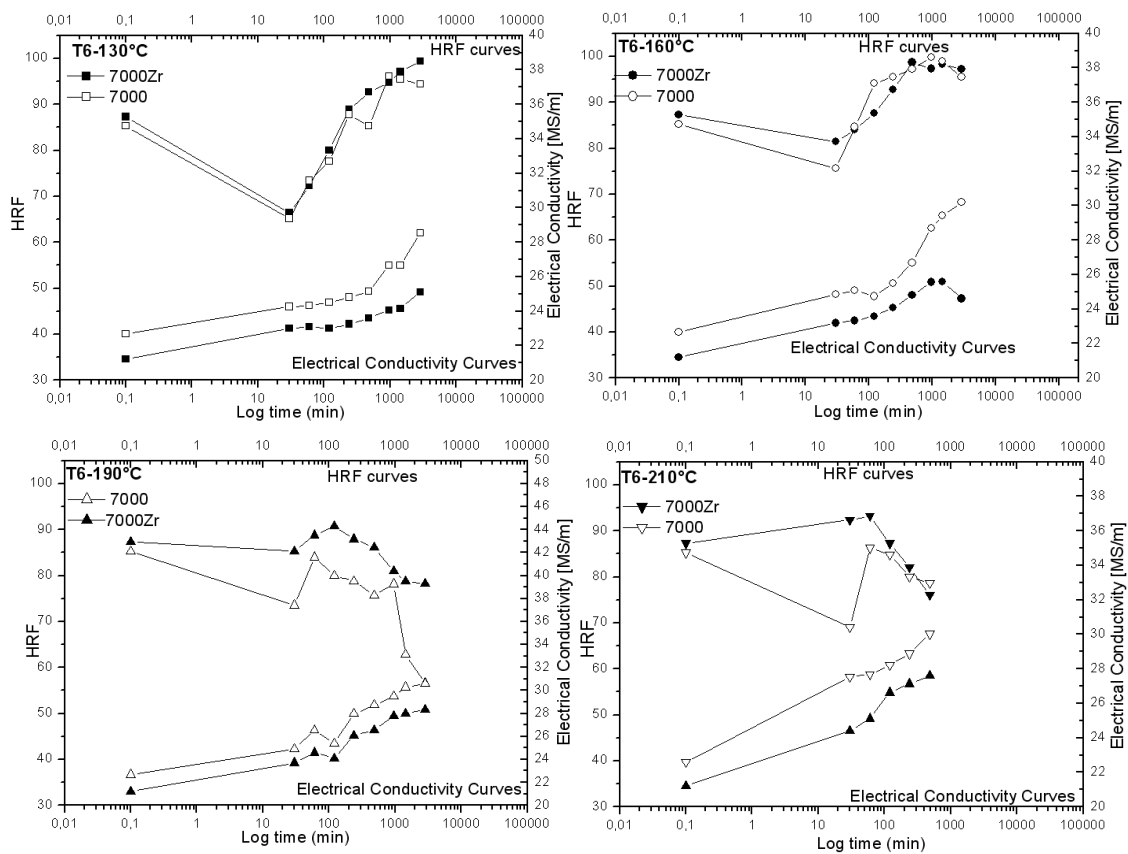


**Figure 4.** Hardness and electrical conductivity of 7000 and 7000Zr alloys during aging at 130°C, 160°C, 190°C and 210°C after solution treatment at 490°C-2h (initial value at 0,1min).

The peak stress  $\sigma_p$  decreases with increasing T at constant  $\dot{\epsilon}$ ; moreover, it decreases with decreasing  $\dot{\epsilon}$  at a fixed temperature [Fig. 10]. For each fixed temperature T, the ductility decreases as  $\dot{\epsilon}$  increases for 7000 alloy deformed by torsion and tension test while rises with  $\dot{\epsilon}$  for 7000 Zr tensile samples. This behavior being more evident with increasing temperature is common in creep [51,52]. In contrast for hot working as  $\dot{\epsilon}$  decreases, ductilities increases since the improved DRV mitigates stress concentration and nucleation of voids (usually at triple junc-

tions). Moreover, at fixed  $\dot{\epsilon}$ , as T increases, recovery is improved and therefore ductility increases. Ductility in torsion is always higher than in tension because the low normal to shear stress ratio enhances the role of DRV in inhibiting cracking [39]. The peak values are always higher in torsion because the higher  $\dot{\epsilon}$  involved. Constitutive analysis for torsion test gave a Q value of 161Kj/mol [1]. The value of Q close to that of pure Al is due to precipitated particles that are inefficient in interacting with dislocations as confirmed by the low declines in the flow curves and by the very low value of average n (1,5)[1]. In fact the microstructure of as-cast samples hot torsioned at temperature higher than 300°C exhibits significant precipitated particles. Their number decrease as T increases do to overaging or cooperative growth of particles and/or to their dissolution while at fixed T increases with strain rate due to strain hardening effect on enhancing precipitation kinetics (Fig. 11). Optical analysis of torsioned samples on longitudinal plane close to fracture surface after chemical etchant (Keller) shows that only the samples deformed at 500°C exhibit recrystallized grains from SRX (Fig. 12). At 400°C the microstructure is characterized mainly by subgrain as is evident from anodized longitudinal plane of Fig.13. Subgrain have been observed in grains at 300°C 0.1s<sup>-1</sup> and 0.01 s<sup>-1</sup> too. Even the samples deformed by tensile at 350°C-400°C show some SRX ( Fig.14). Static recrystallization is much more evident in the alloy without Zr, close to the fracture surface and near grain boundaries and due to stress localization (Fig.14).

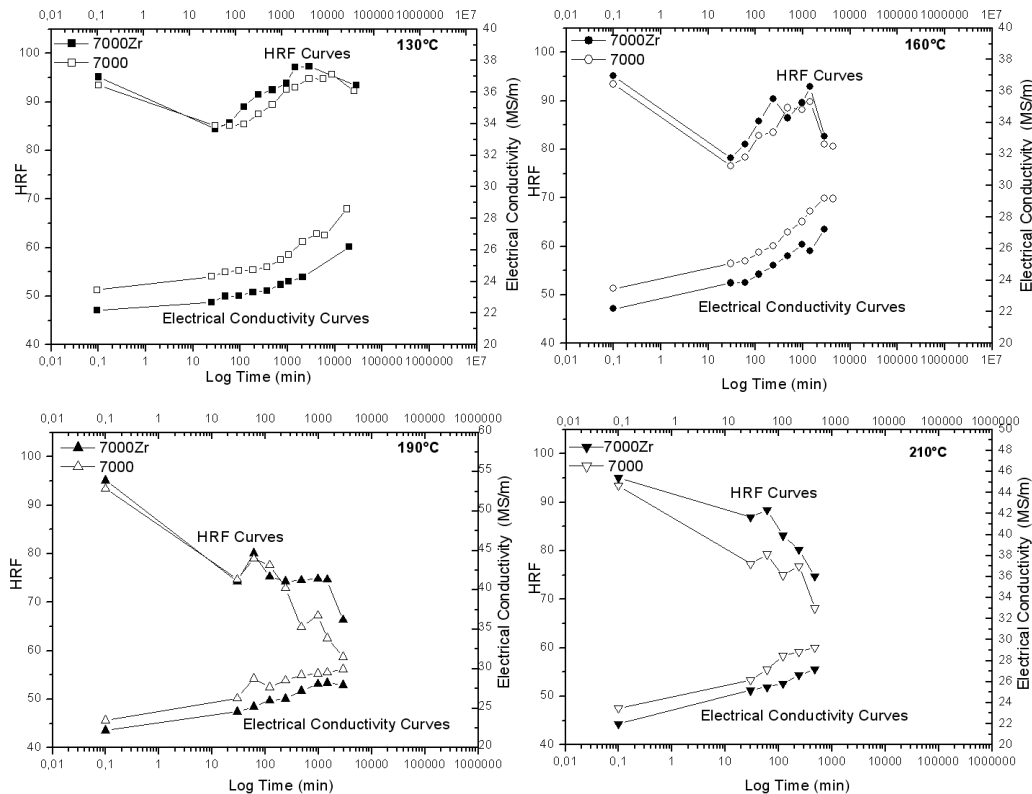


**Figure 5.** Hardness and electrical conductivity of as-cast 7000 and 7000Zr alloys during aging at 130°C, 160°C, 190°C and 210°C (initial value at 0,1 min).

The microstructure of tensioned samples is characterized by cavitation (Fig.15) phenomena. Cavitation is much more evident in the alloy without Zr ( Fig.15 b) and it is strongly reduced only if the alloy is solutionized (490°C-2h) before tensile test (Fig.15c). In fact this phenomena is mainly due to both segregation and stress concentration at particles (Fig.15d). Solution heat treatment reduce microsegregation (Fig.3) and dissolve soluble Mg-Zn particles, leading therefore to a reduction of the both hardness and cavitation. Some brittle particles (for example FeAl<sub>3</sub>/ FeAl<sub>6</sub> in Fig.2) are not dissolved from solution heat treatment and continue to act as cavity nucleation point.

Cavitation (Cs%) Vs strain rate is shown in Fig.16 for as the cast 7000 sample deformed at 250°C and 400°C. Cavitation increases with T and, at fixed T it increases as strain rate decreases. The distribution of cavities along the longitudinal sample surfaces at 250°C and 400°C is shown in Fig. 17. At the lowest T, cavitation values decrease as distance from fracture increases while at 400°C the cavities are randomly distributed along the longitudinal area of the samples. So it can be assumed a more active role of grain boundaries sliding (GBS) on cavitation nucleation and growth at the highest T. Theoretical modelling on cavitation in general takes into account the three distinct stages of damage generation, i.e. nucleation, growth and coalescence [40], but, among these, the growth appears the critical phase [41].

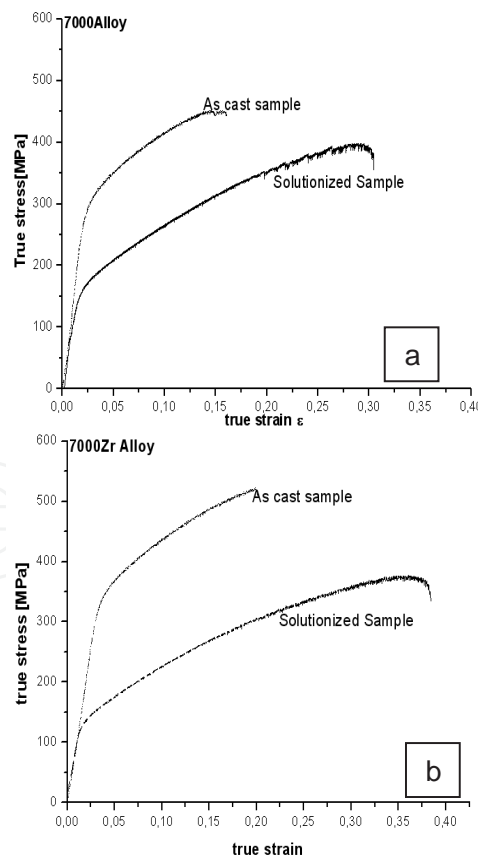


**Figure 6.** Room temperature tensile curves for 7000 (a) and 7000Zr samples (b) in the following conditions: as cast and solution treated 490°C-2h

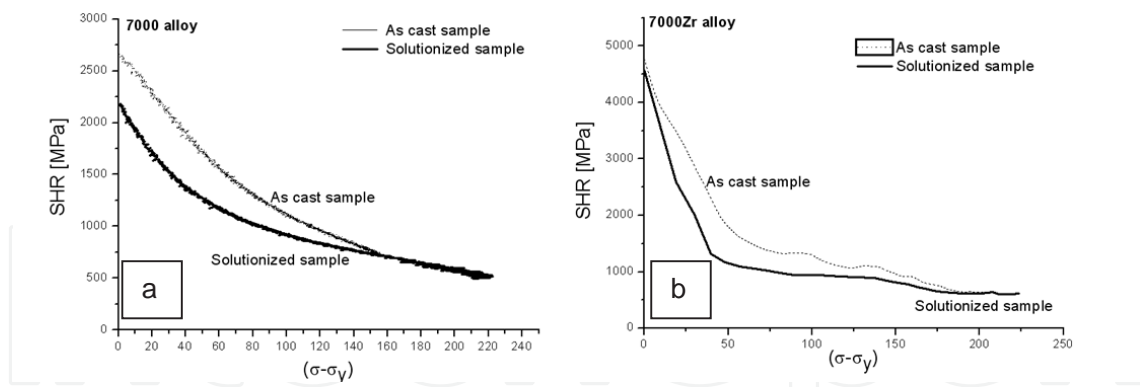


**Figure 7.** Strain hardening rate curves for the RT tensile curves of 7000 (a) and 7000Zr (b) alloy in the as-cast and solutionized state.

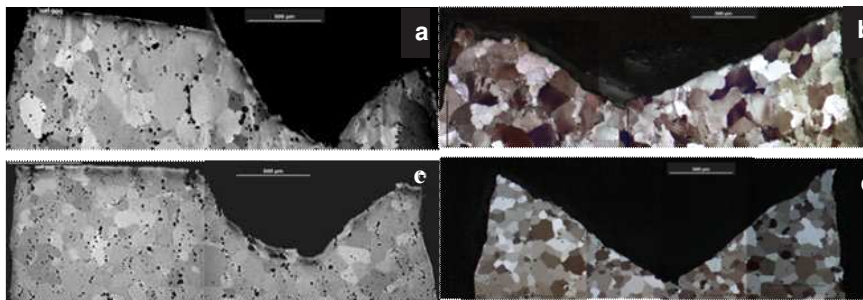


**Figure 8.** Optical micrographs of 7000 tensioned specimens before (a,b) and after 3h of annealing at 500°C (c,d) where (a,c) are as cast, (b,d) are solution treated

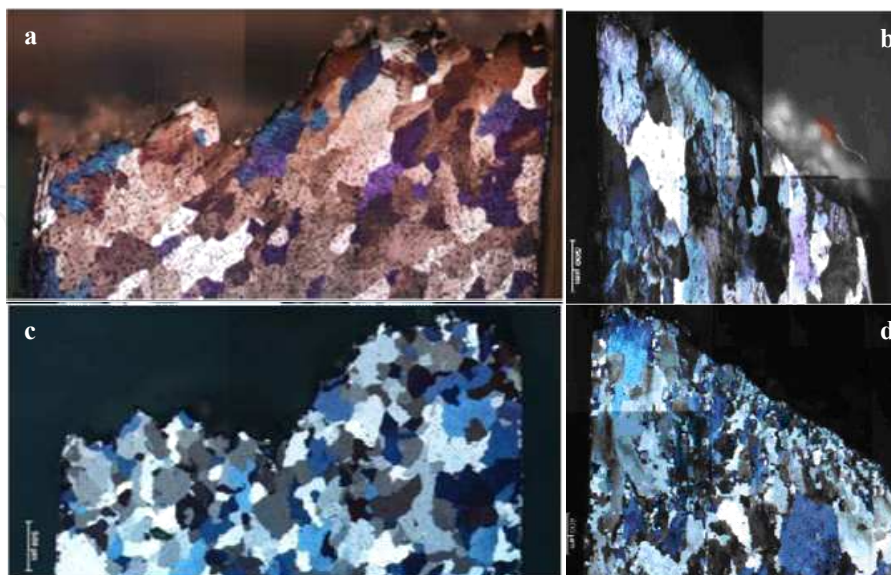


**Figure 9.** Optical micrographs of 7000Zr tensioned specimens before (a,b) and after 3h of annealing at 500°C (c,d) where (a,c) are as-cast, (b,d) are solution treated.

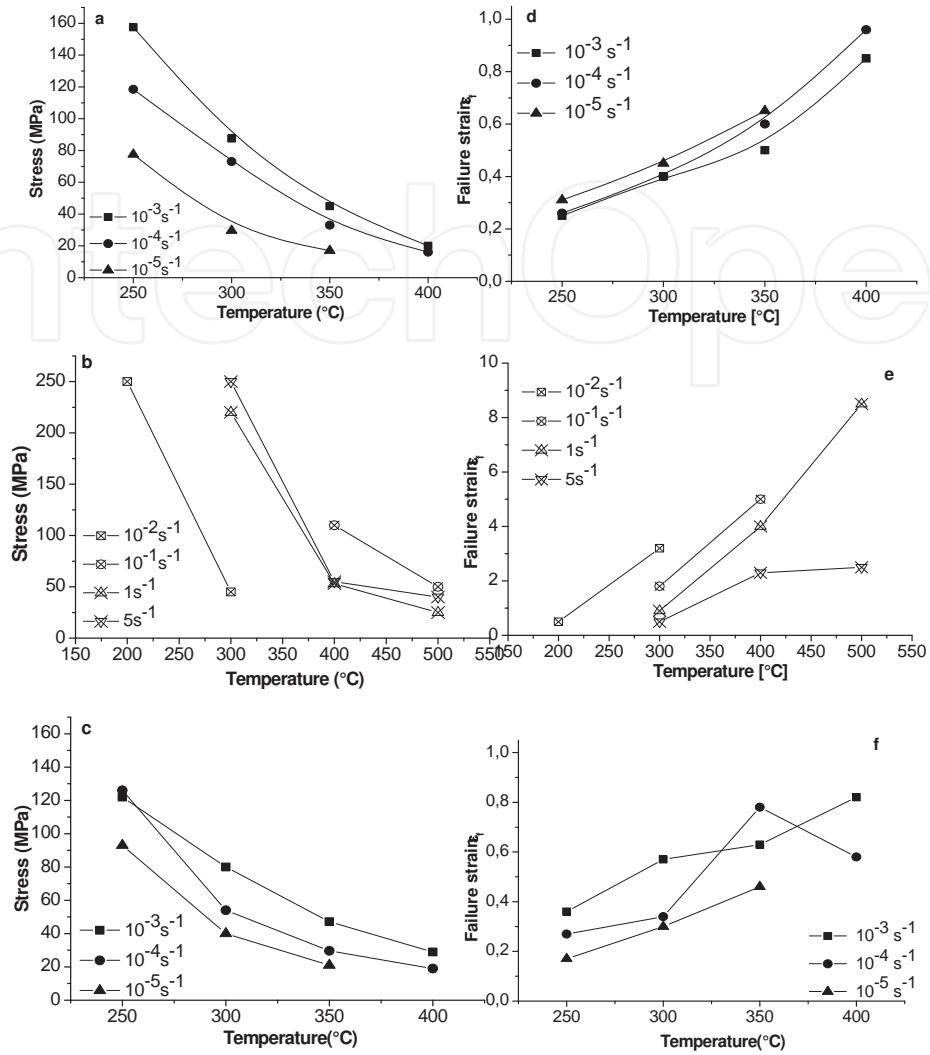


**Figure 10.** Peak stress variations (a,b,c) and failure stress (d,e,f) as a function of T for the as-cast 7000 alloy hot deformed by tension (a,d) and by torsion (b,e) and for 7000 Zr alloy hot deformed by tension (c,f).

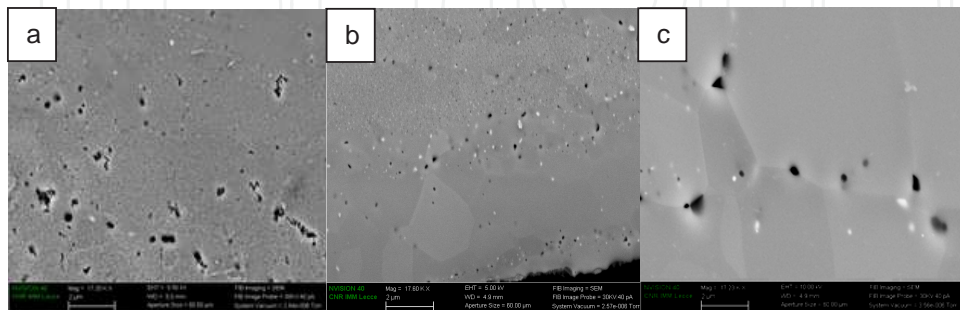


**Figure 11.** Precipitated particles in hot torsioned samples at 300°C-0,1s<sup>-1</sup>(a), 300°C-0,01s<sup>-1</sup> (b) and 400°C-0,1s<sup>-1</sup>(c): at fixed T (a,b) the number of particles increases with strain rate due to enhanced precipitation on dislocations, while as T increases the size of particles increase due to overaging (a,c).

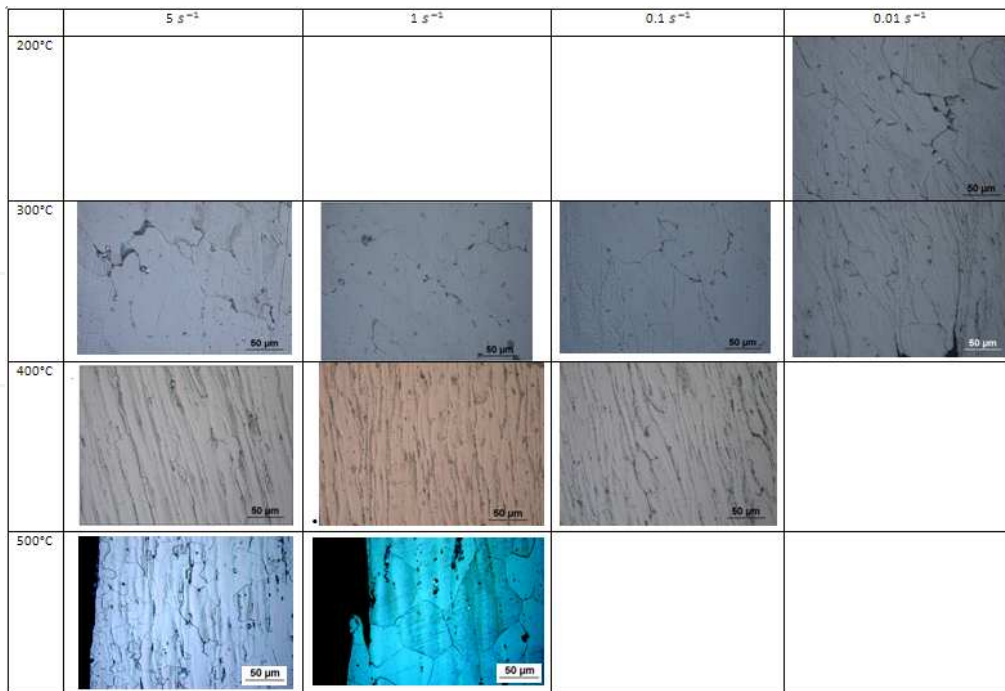


**Figure 12.** Optical micrographs (50X) of torsioned samples on longitudinal planes close to fracture surface after Keller etchant showing that only the samples deformed at the highest T exhibit SRX.

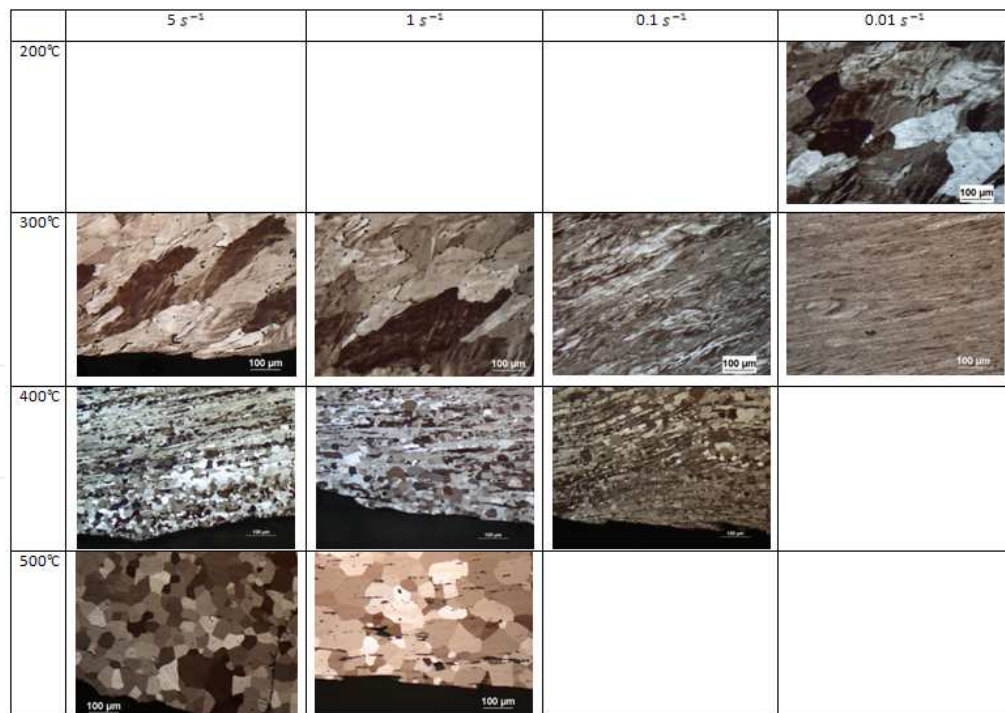


**Figure 13.** Optical micrographs (20X) of torsioned samples on longitudinal planes close to fracture surface after anodizing showing that the microstructure at 400°C and is characterized mainly by subgrains. Subgrains have been observed in some grains at 300°C and  $0.1 \text{ s}^{-1}$ - $0.01 \text{ s}^{-1}$

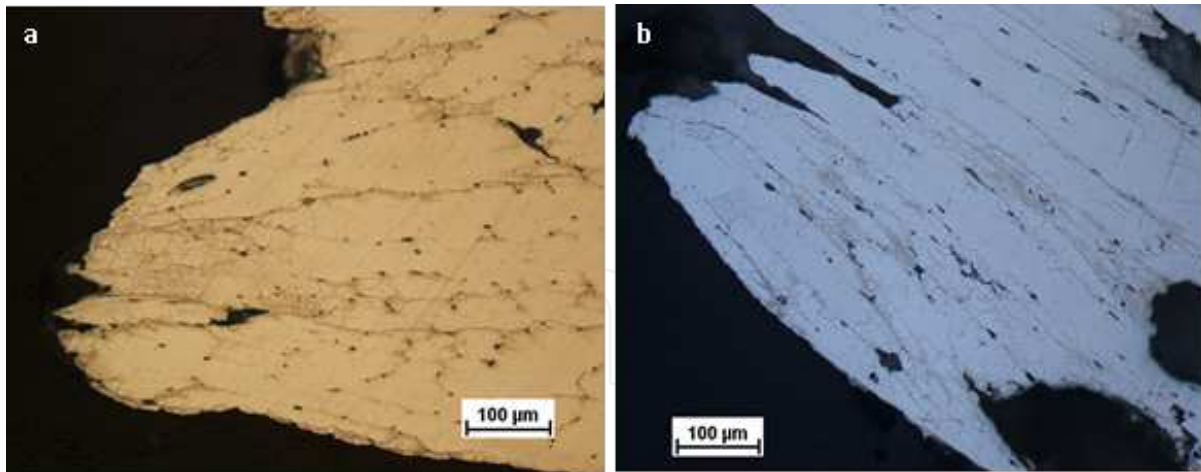


**Figure 14.** SRX close to fracture surface of hot deformed tensile test 7000 alloy at 400°C-10<sup>-4</sup>s<sup>-1</sup> with Zr (a) and without (b)

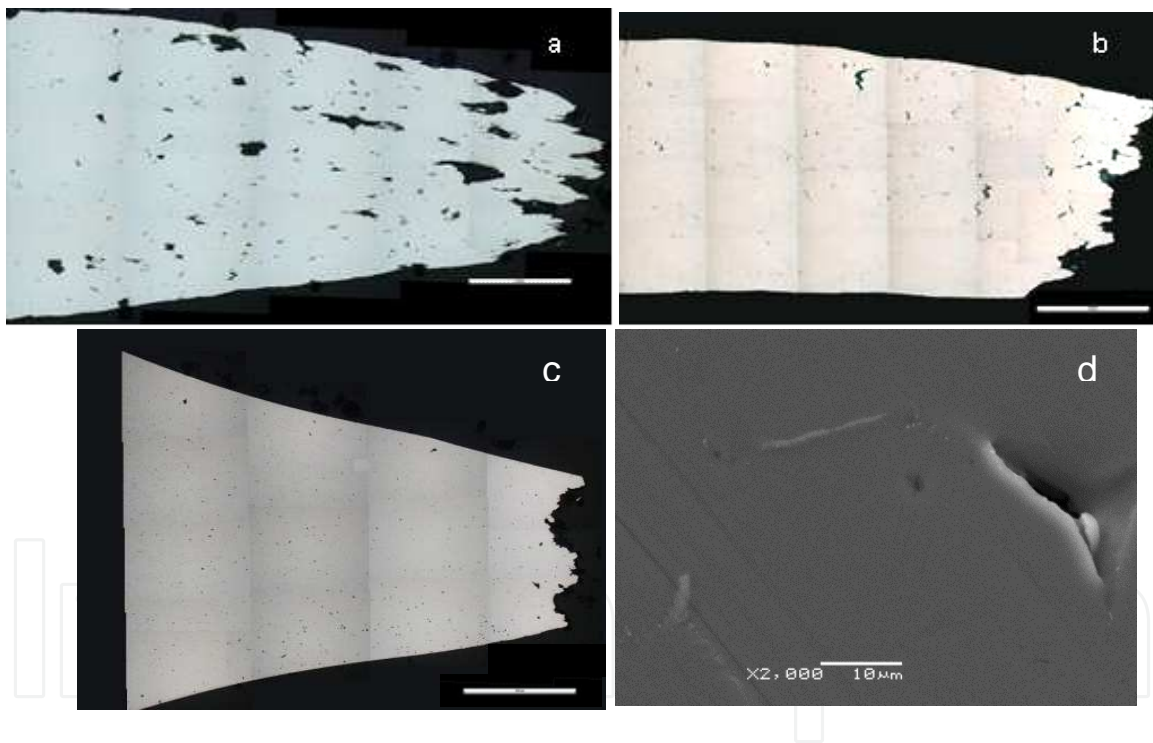


**Figure 15.** Optical micrographs of cavitation phenomena in as-cast 7000 (a), 7000Zr (b), solutionized 7000 alloys (c) deformed by tensile test at 350°C 10<sup>-4</sup> s<sup>-1</sup>. SEM micrographs of 7000 as-cast alloy (d) showing that cavities originate at brittle particles.

When cavity growth is controlled by plastic deformation, the simplest model for cavity growth assumes the following form [38]:

$$C_v = C_0 \exp(\eta \varepsilon) \quad (1)$$

where  $C_0$  is the initial volume fraction of cavities and  $\epsilon$  is the fracture strain. Following Lee and Huang [40], who based their analysis on the Stowell et al. relationship [41], one can express the cavity growth exponent as follows [42]:

$$\eta = \frac{3}{2} \left( \frac{m+1}{m} \right) \sinh \left[ \frac{2(2-m)}{3(2+m)} \right] \quad (2)$$

Where  $m$  is the strain rate sensitivity of flow stress.

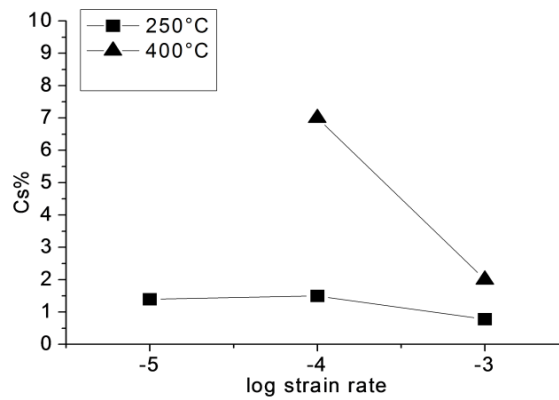


**Figure 16.** Cavitation ( $C_s\%$ ) versus log strain rate showing that the area of fissures increases with  $T$  and, at the highest  $T$ , with decreasing strain rate

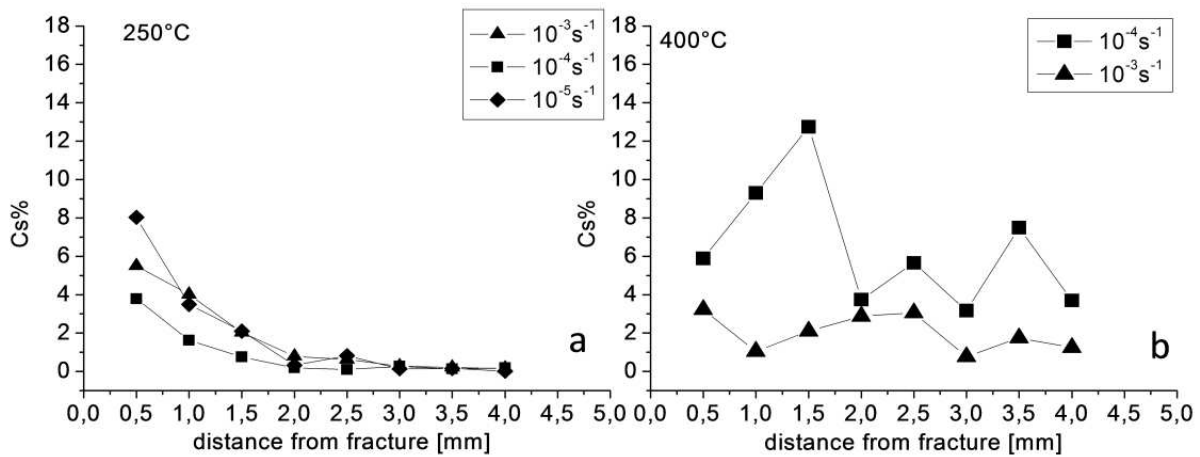


**Figure 17.** Cavitation ( $C_s\%$ ) versus distance from fracture at 250°C (a) and 400°C (b) showing that at the lowest  $T$  the area of fissures decrease as distance from fracture increases while at 400°C cavities are randomly distributed along the longitudinal area of the samples.

When the fracture strain is substituted into Eqn.1, an obvious approximation, since the fracture strain is affected by necking, the plot presented (with  $C_0$  arbitrarily assumed to be

0.03%) in Fig. 18 are obtained. Although this calculation is based on very rough assumptions, the model of cavity growth controlled by plastic strain describes very well the observed cavitation trend. It can be thus reasonably concluded that, in the investigated range of experimental conditions, the cavity growth is mainly driven by plastic straining. GBS substantially contributes to enhance the fraction of cavities at the highest T and justifies the observed difference between the calculated value and experimental one (Fig.18).

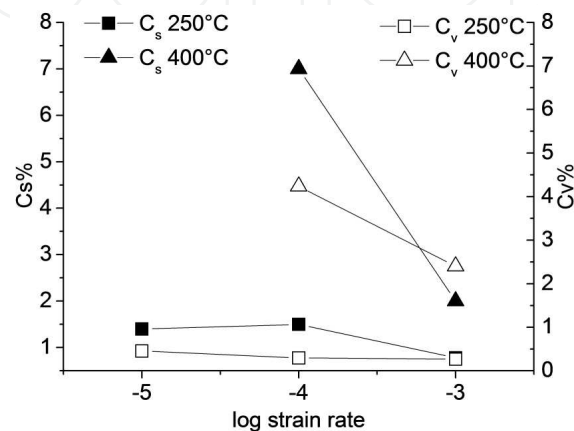


**Figure 18.** Comparison of measured Cs% and calculated Cv% versus log strain rate at 250°C and 400°C

## 4. Conclusions

The main conclusions are summarized in the following :

- In the as received state the grain size of 7000 Zr alloy is larger than that of 7000 alloy due to reaction between Zr and Ti that reduce the nucleation power of both elements and the microstructure of both alloys is characterized by dendritic microsegregation. The solution heat treatment at 490°C-2h leads to a strong reduction of segregation and to a complete dissolution of hardening Al-Zn-Mg particles as shown by EDS analysis. As consequence the hardness decreases. For the larger grain size and higher amount of alloying the electrical conductivity of 7000Zr is always lower than that of 7000 alloy.
- The response to heat treatment for both the as cast and solutionized samples is better at the higher temperature (190°C and 210°C) for the alloy containing Zr, while it is similar for both alloys at the lower temperature of treatment. This behaviour could be due to Al<sub>3</sub>Zr compounds that don't solutionize at high temperature of treatment and moreover, harden the alloy and can act as nucleation sites for hardening precipitate η' phase. Aging treatment of the as-cast alloys for the range of imposed times is ineffective in terms of increasing hardness.

- Concerning RT tensile tests, the SHR is higher for the as cast sample comparing to the solutionized. As consequence the recrystallization rate of as cast sample is faster too. Due to Zr effect it is incomplete and not homogeneous in the Zr modified alloy.
- During hot tensile test the as cast alloys exhibit high flow stress at low temperature due to reduced DRV. At higher T, both improved DRV and overaging of particles lead to reduced peak stress. The phenomena is much more evident during torsion because of T involved. For each fixed temperature T, the ductility decreases as  $\dot{\epsilon}$  increases for 7000 alloy deformed by torsion and tension while rises with  $\dot{\epsilon}$  for 7000 Zr tensile samples.
- The microstructure of both torsion and tensile samples hot deformed at the highest temperatures exhibit some SRX, more evident in the alloy without Zr.
- Cavitation in 7000 hot tensioned samples increases with T and with decreasing strain rate. At the lowest T, 7000 as cast alloy cavitation decreases as distance from fracture surface increases while at the highest T cavities are randomly distributed along longitudinal surface of samples, suggesting a more active role of GBS on cavitation nucleation and growth. Theoretical calculation have shown that cavity growth is mainly driven by plastic straining but GBS substantially contributes to enhance the fraction of cavities and justify the observed difference between the calculated and experimental cavitation values at the highest T and lowest strain rate. Cavitation is reduced if the alloy is solutionized before deformation.

## Author details

P. Leo\* and E. Cerri

Università del Salento, via per Arnesano, Lecce, Italy

## References

- [1] H.J. McQueen, P. Leo and E. Cerri; Aluminum Alloys: Fabrication, Characterization and Applications, : Weimin Yin, Subodh Das, Zhengdong Long Eds: TMS USA 2009 pp.37-44
- [2] J.E. Hatch,ed. Aluminum, Properties, Physical Metallurgy, ASM, Metals Park, Oh, 1984
- [3] H.J.McQueen, O.C. Celliers, Canadian Metal. Quart. 36 (1997), 73-86
- [4] K. Laue, H.Stenger, Extrusion: Process Machinery, Tooling, American Society for Metals, Metals Park, OH (1981), 1-62; 124-152
- [5] Y.Baba, H.Yoshido, Proc. 2nd Intl.Al. Exrusion Tech. Sem., Aluminium Association, Washington, (1997) Vol. 1, 301-306

- [6] T. Engdahl, V. Hansen, P.J. Warren, K. Stiller, *Mater. Sci. Eng. A* 327, (2002), 59
- [7] K. Stiller, P.J. Warren, V. Hansen, J. Angenete, J. Gjonnes, *Mater. Sci. Eng. A* 270, (1999), 55
- [8] S.K. Maloney, K. Hono, I.J. Polmear, S.P. Ringer, *Scripta Mater.* 41, 10, (1999), 1031
- [9] H.Z. Li, V. Hansen, J. Jonnes, L. R. Wallenberg, *Acta Mater.* 47, 9, (1999), 2651
- [10] J.C. Werwinskiold, A. Deschamps, Y. Bréchet, *Mater. Sci. Eng. A* 293, (2000), 267
- [11] M.J. Jones, F.J. Humphreys, *Acta Mater.* 51 (2003) 2149–2159
- [12] H.J. McQueen, N. Owen, *Materials in Automotive Industry* E. Essadigi et al., Eds., *Mat. Soc. Cim*, Montreal (2001), pp. 189–205
- [13] W. Blum, H.J. McQueen, *Aluminum Alloys, Physical Mechanical Properties*, ICAA5 *Mater. Sci. Forum* 217–222, (1996), pp. 31–42
- [14] H.J. McQueen, W. Blum, *Aluminium Alloys, Physical and Mechanical Properties* ICAA6, T. Sato, ed *Japan Inst. Metals* (1998), pp. 99–112
- [15] R.D. Doherty et al. *Mat. Sci. Eng. A* 238, 2 (1997) pp. 219–274
- [16] M. El Mehtedi, S. Spigarelli, E. Evangelista, *La metallurgia italiana*, (September 2007) pp. 21–28
- [17] H.J. McQueen, in *Advanced Materials for 21st Century*, J.R. Weertman Symp, Y.P. Chung Ed, TMS-AIME, Warrendale, PA, (1999), pp. 159–168
- [18] S. Fulop, K.C. Cadien, M.J. Luton, H.J. McQueen, *J. Test Eval.* 5 (1977) pp. 419–426
- [19] N.D. Ryan, H.J. McQueen, *J. Mech. Working Tech.* 12 (1986) pp. 279–296
- [20] C.M. Sellars, W.J. McG. Tegart, *Int. Metall. Rev.* 17 (1972) pp. 1–24
- [21] H.J. McQueen in *Hot deformation of Aluminum alloys*, T.G. Langdon, H.D. Merchant, J.G. Morris and M.A. Zaidi Eds, Warrendale, PA, 1990, pp. 31–54.
- [22] H.J. McQueen and J.J. Jonas in C.Q. Chen et al (eds.), *Aluminum alloys 90 (Icaa2)* Beijing, 1990, pp. 727–742
- [23] H.J. McQueen and K. Conrod in *Microstructural control in Aluminum alloys*, E.H. Chia and H.J. McQueen (Eds), TMS-AIME, Warrendale, PA, 1986, pp. 197–219
- [24] H.J. McQueen, E. Evangelista, J. Bowles and G. Crawford, *Met Sci.* 18, (1984), p. 395–402
- [25] E. Evangelista, H.J. McQueen and E. Bonetti in *Deformation of Multi-phase and particles containing Materials*, J.B. Bildensoren et al (eds), Riso National Laboratory, Roskilde, 1983, pp. 243–250
- [26] H.J. McQueen in *Hot deformation of Aluminum alloys*, T.G. Langdon, H.D. Merchant, J.G. Morris and M.A. Zaidi (eds), Warrendale, PA, 1990, pp. 105–120

- [27] E.Evangelista, A.Forcellese, F. Gabrielli and P.Mengucci in Hot deformation of Aluminum alloys, T.G. Langdon, H.D.Merchant, J.G.Morris and M.A.Zaidi (eds),Warrendale, PA, 1990, pp. 121-139
- [28] B. Verlinden, P.Wouters, H.J. McQueen, E. Aernoudt, L.Delaey and S. Cauwemberg, *Mat.Sci.Eng.A*, 123 (1990) pp.229-237
- [29] P.Wouters, B. Verlinden, H.J. McQueen and E. Aernoudt, *Mat.Sci.Eng.A*, 123 (1990) pp.239-245
- [30] E. Evangelista, E. Di Russo, H.J. McQueen and P. Mengucci in Homogenization and Annealing of Al and Cu Alloys, H.D. Merchant, J. Crane and E.H. Chia (eds.), TMS-AIME Warrendale, PA, 1988, p. 209
- [31] H.J. McQueen, E. Evangelista, A.Forcellese, I.C. Smith and E. Di Russo, in Modelling the deformation of Crystalline Solids, T.C. Lowe, A.D. Rollet, P.S. Follanbee and G.S. Daehn (eds.), TMS-AIME, Warrendale, PA, 1991, p.281-292
- [32] A. Espedal, H. Gjestland, N. Ryum and H.J. McQueen, *Scand J. Met.* 18 ,1989, pp. 131-136
- [33] E. Evangelista, H.J. McQueen and E. Cerri, , Modelling of plastic deformation and its Engineering Applications, S.I. Andersen et al. eds, Riso National Laboratory, Roskilde, DK, 1992, pp. 265-270
- [34] P.A.Friedman and W.B.Copple, Proceeding of TMS,2003,Hot deformation of aluminum alloy III 211-219
- [35] D. Nicolau, S.L. Semiantin, *Acta Mat.* 51, (2003) 613-623
- [36] E.M. Taleff, P.J. Nevland and P. Krajewski, *Metall.Mater.Trans.* 32A (2001) 1119-1130.
- [37] M.F.Ashby, C. Gandhi and D.M.R. Taplin, *Acta Metall.* 27 (1979) 699-729.
- [38] M.J. Stowell, Cavitation in Superplasticity, in "Superplastic forming of structural alloys", N.E. Paton and C.H. Hamilton Eds., TMS-AIME, Warrendale, PA, 1982, 321-326
- [39] H.J.McQueen, *Materials Science Forum*.Vols. 604-605 (2009)
- [40] X.-G. Jiang, J.C. Erathman and F.A.Mohamed, *J.Mater.Sci.* 29 (1994) 5499-5514.
- [41] C.J.Lee and J.C.Huang, *Acta Mater.* 52 (2004) 3111-3122.
- [42] M.J.Stowell, D.W.Livesey and N.Ridley, *Acta Metall.* 32 (1984) 35-42.
- [43] J. Polmear Light alloys –Metallurgy of light metals, Butterworth Heinemann 1995, 115-118
- [44] Bjorn Ronning, Thesis " Constitutive relationships for AlZnMg, AlZnMgCr and AlZnMgZr alloys" October 1998, University of Trondheim, Norway

- [45] P. Leo, E. Cerri, H.J. McQueen and S. Chiozzi, *Mater. Sci. Forum* 604-605; 2009, pp. 67-76
- [46] L.K. Berg, G. Gjonnes, V. Hansen et al. *Acta Mater*, 49, (2001), 3493
- [47] H. Loffer, I. Kovacs, J. Lendvai, *J. Mater. Sci.* 18, (1983), 2215
- [48] Z. Katz, N. Ryum, *Scripta Met.* 15, (1981), 265
- [49] J.D. Verhoeven, "Fundamental of Physical Metallurgy" J. Wiley e Sons, NY (1975), Chapter 6,
- [50] P. Leo, E. Cerri, H. McQueen and A. Taurino, ICA11, in 'Aluminium Alloys – Their Physical and Mechanical Properties' J. Hirsch, B. Skrotzki and G. Gottstein eds, Wiley-VCH (DE) 2008, pp. 1868-1874.
- [51] M.E. Kassner, M.T. Perez-Prado, *Fundamental of creep in metals and alloys*, Elsevier 2004, 1-15
- [52] R.W. Evans, B. Wilshire, *Introduction to creep*, Oakdale Printing Company Ltd, 1993, 16-22

